Eur. Phys. J. Plus (2024) 139:346
https://doi.org/10.1140/epjp/s13360-024-05151-w

THE EUROPEAN PHYSICAL JOURNAL PLUS

Regular Article

Structural and optical properties of Eu^{3+}-doped sol–gel silica–soda glasses

Francesco Enrichi[1,2,a], **Gabriella Mastantuoni**[3], **Michele Cassetta**[1,4], **Alessia Sambugaro**[1], **Nicola Daldosso**[1], **Alessandro Martucci**[5], **Alberto Vomiero**[6,7], **Elti Cattaruzza**[6], **Giancarlo C. Righini**[8]

[1] Department of Engineering for Innovation Medicine, University of Verona, Strada Le Grazie 15, 37134 Verona, Italy
[2] ISP-CNR Institute of Polar Sciences - National Research Council, Via Torino 155, 30172 Mestre-Venice, Italy
[3] Division of Glycoscience, Department of Chemistry, School of Engineering Sciences in Chemistry, Biotechnology, and Health, KTH Royal Institute of Technology, AlbaNova University Centre, 106 91 Stockholm, Sweden
[4] Department of Industrial Engineering, University of Trento, 38122 Trento, Italy
[5] Department of Industrial Engineering and INSTM, University of Padova, 35131 Padua, Italy
[6] Department of Molecular Sciences and Nanosystems, Ca' Foscari University of Venice, Via Torino 155, 30172 Mestre-Venice, Italy
[7] Division of Materials Science, Department of Engineering Sciences and Mathematics, Luleå University of Technology, 97187 Luleå, Sweden
[8] IFAC-CNR "Nello Carrara" Institute of Applied Physics – National Research Council, MiPLab, Via Madonna del Piano 10, 50019 Sesto Fiorentino, Italy

Received: 29 October 2023 / Accepted: 3 April 2024

Abstract Rare earths (REs) incorporated in glasses, mostly in the form of RE^{3+} ions, have several applications such as lasers and optical amplifiers, spectral conversion layers for solar cells, light emitters and sensors. In this context, both the composition and the structural properties of the glass, as well as the dopant concentration play an important role in determining the optical properties and the efficiency of the system. Usually, the concentration of REs is small, below 1 at%, to avoid clustering and optical quenching. In this paper, we report the case of sol–gel Eu-doped silica–soda glass films. The addition of soda to silica can reduce RE clustering and precipitation, according to molecular dynamic simulations, but brings structural instabilities to the network. Here, sodium was varied from 10 to 30 at% and Eu from 0 to 8 at%. It was shown that Eu plays a significant role in the stabilization of the matrix, improving the transparency, the refractive index and the thickness of the films. The increase of Eu concentration provides a decrease of site symmetry and an increase of quantum efficiency (QY), reaching 71% for the highest 8 at% Eu doping, with remarkable absence of concentration quenching.

1 Introduction

Rare-earth ions (RE^{3+}) incorporated in glasses have several applications in optics and photonics. They are used in lasers and optical amplifiers [1, 2], spectral conversion layers for solar cells [3–8], as emitters in solid-state lighting [9] and sensors [10]. Sol–gel films are particularly interesting for these applications because of their versatility and high optical quality. They can be easily deposited as coatings for spectral conversion and they offer the possibility to realize optical waveguides for photonics. The peculiar properties of RE^{3+} ions are related to a wide range of electronic transitions within the 4*f* orbitals, characterized by narrow absorption and emission wavelengths from the UV to the infrared, possibility of multi-photon absorption and emission resulting in up-conversion and down-conversion processes, long luminescence lifetimes [11]. The glassy matrix provides a versatile environment for incorporating RE^{3+} ions, due to the workability of this material and the possibility of fine tuning its composition. The final optical properties depend on the concentration of the dopants as well as on the chemical environment of the host material. Silica as single-oxide glass is known to be one of the worst host materials for REs since the network structure fails to accommodate a great number of RE atoms without clustering. This was firstly reported for neodymium [12] and then for erbium [13], demonstrating that other elements such as Na, Al and P should be included in the glass composition to facilitate RE incorporation minimizing RE aggregation by tailoring the chemical, elastic, mechanical and viscous properties [14, 15]. Based on these observations, structural studies of the local environment around RE ions [16, 17] suggested a model in which co-dopants form a solvation shell around the RE ions that is able to dissolve and disperse them homogeneously in the glass matrix while providing well coordination ligands. Indeed, molecular dynamic simulations previously done on Er-doped glasses allowed to understand the role of sodium and aluminum in their accommodation and dispersion. Therefore, we focused on silica–soda for the better capacity of dispersing RE elements. Europium was selected as dopant both for its capability to stabilize the network instabilities of these glasses and for its characteristic optical emissions due to $^5D_0 \rightarrow {}^7F_J$ ($J = 0$–6) transitions. Unlike other RE^{3+} ions, Eu^{3+} luminescence is sensitive to the local environment around it and can be used as a local probe [18–22], providing information about the site symmetry around it. Moreover, Eu^{3+} radiative lifetime can be calculated by the

[a] e-mail: francesco.enrichi@univr.it (corresponding author)

Published online: 24 April 2024

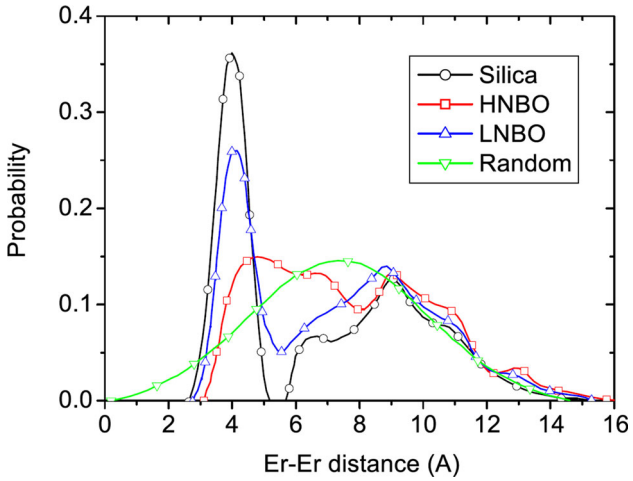

Fig. 1 Simulated distribution of distances between Er atoms (0.9 mol% of Er_2O_3) in different matrices: SiO_2 (Silica), SiO_2/Na_2O (HNBO), $SiO_2/Al_2O_3/Na_2O$ (LNBO). A random distribution is also reported for comparison. (Reproduced from [25])

PL emission spectral shape without the need for absorption analysis, and therefore, the quantum efficiency can be straightforwardly obtained by rating the measured lifetime to the radiative one [23, 24]. These features make Eu^{3+} a unique tool for the study and optimization of the whole system. Na and Eu concentrations were both varied to deeper understand the interrelations between the structural and the optical properties of the glassy material.

2 Local structure of RE^{3+} ions in multicomponent glasses

It is worth recalling previous results on the role of sodium and aluminum within the silica glass network in relation to the clustering and precipitation of rare earth elements. To better understand the impact of the glass composition on the REs distance distribution, molecular dynamics was used with a model of 5128 atoms [25]. Three representative glass compositions were investigated: silica (SiO_2) (S), alkali silicates (SiO_2–Na_2O) (HNBO) and aluminosilicates (SiO_2–Al_2O_3–Na_2O) (LNBO). The glasses are different by the number (H = high; L = low) of non-bridging oxygens (NBO) and their structure at NBO constant. The RE oxide concentration was 0.9 mol% which corresponds, depending on the glass density, to $4 \div 6 \times 10^{20}$ ions/cm^3. Although those simulations were performed on Er^{3+} ions, the same results can be transferred to other rare earth atoms due to their similar chemical properties.

In Fig. 1, the distributions of minimum distance between Er atoms in the three hosts are shown. A random distribution of erbium atoms at the same concentration is also reported for comparison. At this Er concentration, the average distance between erbium atoms in a random system is around 7 nm. In silica, the distribution is split in two with more than 47% of erbium being clustered (the cluster average distance is 4 nm). Adding alkali (Na) to silica significantly drops the cluster peak at 4 nm and the erbium distribution looks like a random one (HNBO curve). This can be explained by the fact that alkali break the network by creating NBO which can easily accommodate the erbium ions [13, 16, 17]. If now we add alumina to the previous glass such as Al/Na = 1 (LNBO curve) we are in a situation quite similar to silica in terms of NBO since at that ratio NBO = 0. However, due to structural differences (presence of alumina) the clustering is certainly higher than the HNBO glass but lower than the silica one. Silica therefore is the worst host for accommodating high erbium concentrations without clustering, HNBO are the best and LNBO are intermediate. These results agree with studies on europium in silica and sodium silicate glasses [26]. That is why we focused our research on a silica–soda HNBO system.

3 Theoretical overview of Eu^{3+} spectral properties

The spectra of RE^{3+} ions correspond to intra-4*f* orbital transitions, having mainly electric dipole character. For a free ion, electric dipole transitions between states of the same configuration are parity forbidden. In solids or solutions, the occurrence of non-centrosymmetric interactions with the surrounding atoms leads to a mixing of states of opposite parity. This mixing may result from several distinct mechanisms, one of the majors being the coupling of states of opposite parity by way of the odd terms in the crystal field expansion [21]. The radiative transitions from an excited state to lower lying states give rise to several lines in the emission spectrum, whose intensities are related to the spontaneous emission probability, therefore to the dipole strength of the specific transition. In the trivalent RE ions, the transitions of interest consist mainly of weak magnetic dipole (MD) and induced electric dipole (ED) transitions. The intensities of the MD transitions are not influenced by the chemical environment of the ion, whereas those of the ED transitions are quite sensitive to it.

In 1962, Judd [27] and Ofelt [28] independently developed a model for the calculation of the oscillator strengths of lanthanide electric dipole *f–f* transitions. Judd–Ofelt theory has been very successful in understanding and predicting the spectral intensities, especially for ions in inorganic glasses and crystals.

The red luminescence of Eu^{3+} is a result of the transitions from its $^5D_0$ state to the lower lying ^7F_J levels ($J = 0$–6). The transitions from $^5D_0$ to $^7F_{0,3,5}$ are forbidden both in magnetic and induced electric dipole schemes. The transition to $^7F_1$ is the only magnetic dipole contribution. Magnetic dipole transitions in lanthanide ions are practically independent of the ion's surroundings and can be well calculated by theory. The remaining transitions to $^7F_{2,4,6}$ are purely of induced electric dipole nature. According to the Judd–Ofelt theory, the strength of all induced dipole transitions (absorption and emission) of a lanthanide ion in a certain matrix can be calculated on the basis of only three parameters which are usually determined experimentally.

Transitions arising from the $^5D_0$ level of the Eu^{3+} electronic configuration are easily assigned by the theory. The first important observation concerns the relative transition intensities between the electric dipolar $^5D_0 \rightarrow {}^7F_2$ (about 610 nm) and the magnetic dipolar $^5D_0 \rightarrow {}^7F_1$ (about 590 nm) transitions:

$$R = \frac{I\left({}^5D_0 \rightarrow {}^7F_2\right)}{I\left({}^5D_0 \rightarrow {}^7F_1\right)} \tag{1}$$

The higher this ratio, the lower the local symmetry around Eu^{3+} is with respect to an inversion center, since a high local symmetry strongly reduces the electric dipolar emission without affecting the magnetic dipolar one, and vice versa.

Another unique property related to the internal ^4f transitions of Eu^{3+} ions as depicted by the Judd–Ofelt analysis is that the intensity of the $^5D_0 \rightarrow {}^7F_1$ transition, being magnetic dipolar in character and therefore insensitive to change in the Eu^{3+} surroundings, may be taken as a reference, with a radiative rate of 50 s^{-1}. All the other observed transitions arising from the $^5D_0$ level have an electric dipolar character. Therefore, assuming the occurrence of only radiative and non-radiative processes in the depopulation of the $^5D_0$ excited level, from these two intensity ratios the $^5D_0$ radiative lifetime can be evaluated. From a practical point of view, the radiative lifetime (τ_{RAD}) can be calculated by the following equation:

$$\left(\frac{1}{\tau_{\mathrm{RAD}}}\right)_{\mathrm{Eu}} = 14.65n^3 \frac{I(^5\mathrm{D}_0 \rightarrow {}^7\mathrm{F}_J)}{I(^5\mathrm{D}_0 \rightarrow {}^7\mathrm{F}_1)}, \tag{2}$$

where n is the refractive index, $I(^5D_0 \rightarrow {}^7F_J) / I(^5D_0 \rightarrow {}^7F_1)$ is the ratio between the total integrated emission from the Eu $^5D_0$ level to the ^7F_J manifold ($J = 0$–6) and the integrated intensity of the transition $^5D_0 \rightarrow {}^7F_1$ [23, 24].

Therefore, by comparing the experimental lifetime τ_{EXP} with the radiative lifetime calculated from the luminescence emission spectra τ_{RAD} it is possible to give an evaluation of the quantum efficiency QY of the emitting Eu^{3+} ions:

$$QY = \frac{\tau_{\mathrm{EXP}}}{\tau_{\mathrm{RAD}}} \tag{3}$$

Both the symmetry and the quantum efficiency of Eu^{3+}-doped silicates provides fundamental information for the development of the best optical emitting material. However, limited studies are available in the literature and the issue will be systematically investigated here.

4 Experimental

Eu^{3+}-doped silica–soda glasses were synthesized by a sol–gel procedure. Tetraethyl orthosilicate $Si(OC_2H_5)_4$ (TEOS) [Sigma-Aldrich] and $Na(CH_3COO)$ (NaAc) [Sigma-Aldrich] were used as precursors for silica and soda, respectively. Eu^{3+} doping was obtained by adding proper concentrations of the nitrate hydrate $Eu(NO_3)_3 \cdot 5H_2O$ [Sigma-Aldrich]. TEOS was dissolved in ethanol (EtOH) and hydrolyzed with H_2O and HCl (TEOS:HCl:H_2O:EtOH = 1:0.01:2:40). NaAc and $Eu(NO_3)_3$ were dissolved in 1 ml of methanol and ethanol, respectively. These solutions were added to the previous solution and left stirring overnight. The quantities of Eu in different samples ranged from 0 to 8 at%, keeping 20 at% Na. The amount of Na was also changed from 10 to 30 at%, keeping 5 at% Eu. Multilayer films (10 layers) were deposited on fused silica substrates by dipping in dry atmosphere (humidity below 20%). Each layer was annealed in air at 800 °C for 10 min. A final heat treatment in air at 800 °C for 1 h was performed after the deposition of the last layer.

Compositional, morphological, structural and optical characterization of the films were obtained by Rutherford Backscattering Spectrometry (RBS), ellipsometry, UV–Vis spectroscopy and photoluminescence spectroscopy (PL).

RBS was carried out by using a 2.2 MeV $^4He^+$ beam at 160° backscattering angle in IBM geometry. RUMP code was used for the analysis of the experimental spectra [29]. The conversion from areal density (the natural unit of measurement for RBS) to film thickness is based on a film density of 2.65 g cm^{-3}, a typical value for a soda–lime silicate glass.

Ellipsometry quantities Ψ and Δ were measured using a J.A. Woollam V-VASE Spectroscopic Ellipsometer in vertical configuration, at three different angles of incidence (50°, 60°, 70°) in the wavelength range 300–1000 nm. The refractive index n and extinction coefficient k were evaluated from Ψ, Δ and using WVASE32 ellipsometry data analysis software considering a Cauchy dispersion model.

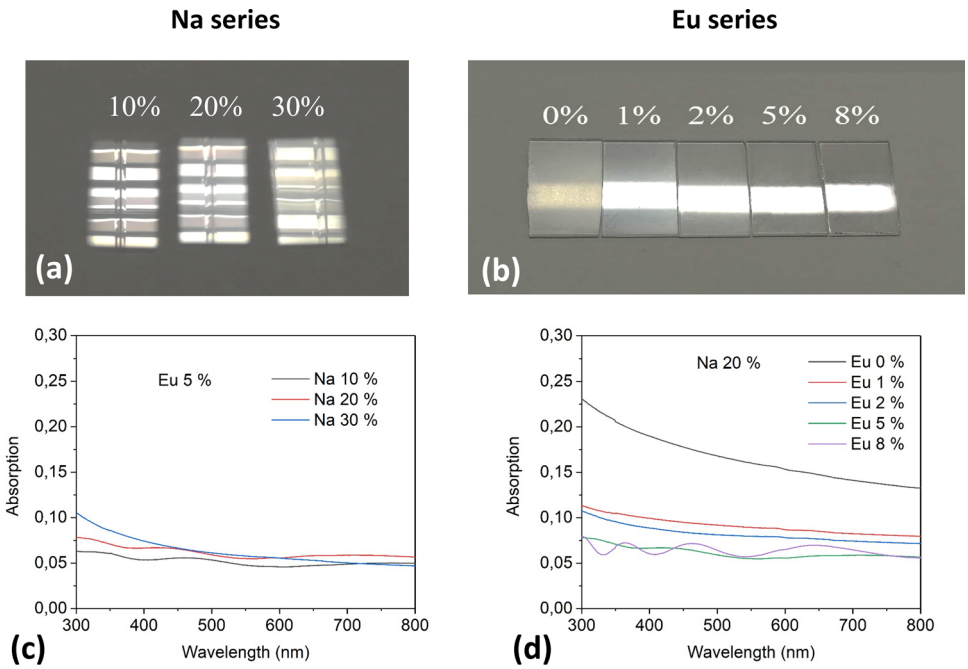

Fig. 2 Optical image under visible light of the Na series with 5 at% Eu (**a**) and Eu series with 20 at% Na (**b**). Increasing the amount of Na, as well as decreasing the amount of Eu, brings a milky appearance with worsening of the transparency. A transparent sample is obtained above 5 at% Eu, when Na is below 20 at%. This is further attested by UV–Vis absorption spectra, reported in (**c**) and (**d**) for Na series and Eu series, respectively. Interference fringes indicate a good transparency of the films, while for Na above 20 at% and Eu below 5 at% the wavelength dependence follows the typical Mie scattering for inhomogeneities size $d >> \lambda$

Absorbance spectra were obtained in transmission with a Cary 5000 UV–Vis-NIR spectrophotometer (Agilent Technologies) between 300 and 800 nm.

Photoluminescence excitation (PLE) and emission (PL) spectra were collected by an Edinburgh Instruments FLS980 Photoluminescence Spectrometer. A continuous-wave xenon lamp was employed as excitation source for steady-state measurements; for wavelength selection, it was coupled to a double-grating monochromator. Time-resolved measurements were obtained in multichannel scaling (MCS) mode, exciting the sample with a pulsed xenon flash lamp with pulse duration of 1 μs and repetition frequency of 10 Hz. The emitted light from the sample was collected by a double-grating monochromator and recorded by a PMT R928P photomultiplier tube cooled at − 20 °C (for measurements in the UV region up to 800 nm).

5 Results and discussion

Different silica–soda samples were prepared by varying both Na content from 10 to 30 at% (Eu fixed at 5 at%) and Eu amount from 0 to 8 at% (Na fixed at 20 at%) with respect to Si.

In Fig. 2a, the optical images under visible light are reported for Na series. Increasing the amount of Na brings a worsening of the transparency, clearly shown by the lamp reflections on the samples. A similar comparison is shown in Fig. 2b for Eu series. Eu content has a major impact on the final characteristics of the deposited films. The transparency of the films before exchange is significantly improved by increasing Eu, in particular for 5 and 8 at%, as shown by the lamp reflections. Before discussing a detailed explanation of this behavior, it is worth presenting the experimental results of UV–Vis, ellipsometry and RBS.

Indeed, these qualitative observations are confirmed by UV–Vis absorption, reported in Fig. 2c and d for Na and Eu series, respectively. The transparent samples exhibit typical interference fringes characterized by intensity oscillations. The highest optical quality is obtained for Na20Eu8 sample. With increase in Na content or decrease in Eu content, the samples assume a milky aspect, and the absorption spectra change to the typical Mie scattering dispersion curve, indicating in homogeneities and defects in the network with size $d >> \lambda$. To further support this point, the scattering curves were fitted by the following equation:

$$\mathrm{Abs}(\lambda) = A + \frac{B}{\lambda^C} \tag{4}$$

where A accounts for the baseline due to surface reflection, B is a normalizing parameter, and C is the scattering exponent of the curve. Rayleigh scattering, due to particles with size $d << \lambda$ is known to have an exponent $C = 4$. For Mie scattering, the curve is much flatter, as described in many theoretical and experimental studies [30–32]. Values in our samples obtained by a Levenberg–Marquardt fitting procedure were the following: Na30Eu5 (2.16 ± 0.02), Na20Eu0 (0.96 ± 0.01), Na20Eu1 (0.82 ± 0.02), Na20Eu2 (1.99 ± 0.03). It should be noted that values around 1 were observed for the most scattering samples Na20Eu0 and Na20Eu1, while values around 2 were observed for samples Na30Eu5 and Na20Eu2. The different exponent values can be reasonably attributed to the different size distribution of the scattering elements. Indeed, Rayleigh and Mie scattering occur simultaneously in the medium depending on

Table 1 Ellipsometry analysis on selected transparent samples

Sample	Thickness D (nm)*	Refractive index n @ 600 nm	Extinction coefficient k @ 600 nm
Na10Eu5	360 (320)	1.489	0.0305
Na20Eu5	370 (315)	1.496	0.0315
Na20Eu8	540 (415)	1.512	0.0161

The thickness, the index of refraction and the extinction coefficient are reported. Relative uncertainty for thickness is about few %, for the other two physical quantities is less than 1%

*In brackets, thickness values from RBS are observed. Uncertainty is about 5 nm

the size of the scatterers. When the size decreases, the film is more transparent and we can expect a higher scattering exponent as observed in our samples.

Ellipsometry analysis was performed on selected transparent samples to get information about the thickness of the films and the optical index of refraction and extinction. The data, reported in Table 1, show a major role of Eu doping in increasing the thickness and refractive index of the samples. A thickness comparison among the samples has been performed also by RBS analysis and will be discussed later. The increase in refractive index is commonly observed in amorphous glasses when RE^{3+} ions are added to the composition [33, 34]. Finally, the extinction coefficients are in perfect agreement with the previous UV–Vis absorption measurements.

An extended RBS analysis was done on all the samples aiming at studying the in-depth composition of the films, doping concentration and thickness. The experimental results confirmed that the average compositions agree with the nominal values of Si, Eu and Na. The difference between ellipsometric and RBS thickness determinations reported in Tab. 1 may be related to the assumption (for RBS) of a bulk soda–lime glass density for the deposited film; actually, our silica–soda sol–gel films have certainly a smaller density (depending on the degree of condensation of the sol–gel process), thus justifying the systematic underestimation of the film thickness by RBS. If we start by the ellipsometric thickness evaluation and we use RBS data to estimate the film density, we obtain 2.35, 2.25 and 2.05 g cm^{-3} for Na10Eu5, Na20Eu5 and Na20Eu8 film, respectively (uncertainty around 0.05 g cm^{-3}).

It is worth observing that elemental diffusion was seen in samples with high Na concentration or low Eu concentration. The effect of Na in glasses and its self-diffusion is well known in the literature. Studies on binary silica–soda glasses showed that the introduction of Na_2O leads to the breaking of the Si–O–Si bonds and the weakening of the silicon–oxygen network. As a result, to a first approximation, the diffusion coefficient increases exponentially with an increase in the concentration of the alkali oxide [35, 36]. This factor can explain the observed migration of the dopants toward the surface in silica–soda glasses during the multilayer deposition process. However, the opposite trend occurs when increasing Eu concentration from 0 to 8 at%, providing a transparent and flat surface above 5 at%. Increasing Eu reduces or stops diffusion, as observed by a uniform distribution of the dopants. This behavior can be explained by looking at molecular dynamic simulations on RE-doped silica and silica–soda glasses, as discussed earlier, which provides detailed investigation of the surrounding environment for the rare earth ion [25, 26]. It was found that RE ions have different coordination numbers in the two glasses. Due to the driving force to satisfy the coordination requirements of non-bridging oxygen to balance the charge, RE ions tend to segregate to form clusters in pure silica, so they can share non-bridging oxygen ions. Instead, in silica–soda glasses there are abundant non-bridging oxygen ions to be charge balanced by Eu^{3+}. Because these NBOs provide an easier way to satisfy the coordination requirements of Eu ions, they do not need to form clusters and they act as stabilizers for the network structure. It is worth noting that the increasing loss of transparency matches with the well-known phase separation process occurring for composition between $10 \div 30$ at% of Na ($5 \div 15$ mol% Na_2O) at about 800 °C [37] or during the consolidation process of the sol–gel [38]. Conversely, the introduction of a charge balancer (Eu^{3+}) reduces this effect suppressing unwished light scattering and discontinuities in the refractive index.

The results for film thicknesses obtained by RBS, anticipated in Table 1 for a few selected samples, are reported in Table 2. The thickness was evaluated by looking at Eu profile; therefore, it was not possible to obtain a reliable value for the lower doped samples. As already discussed, the comparison with ellipsometry denotes a systematic thickness underestimation by RBS, which can be attributed to the assumption of a dense soda–lime film.

In agreement with ellipsometry, the thickness of the films was found to increase with Eu doping concentration. To understand the relation between Eu concentration and film thickness, we need to point the attention on the sol–gel process, where the precursor for Eu is europium nitrate pentahydrate. Increasing the concentration of europium provides higher amounts of nitrate, which lowers the pH of the solution, making it more acidic. Indeed, it dissociates in water releasing (Eu^{3+}) and nitrate ions (NO_3^-). The nitrate ions hydrolyze in water in nitric acid (HNO_3) and hydroxide ions (OH^-). The hydroxide ions then react with the metal alkoxide precursor to initiate the sol–gel reaction, while the nitric acid increases the acidity of the sol, lowering its pH. As a result, in the sol–gel process, hydrolysis becomes more dominant than condensation. The lower level of condensation results in a more porous gel network, and the different composition modifies the viscosity of the solution. Moreover, RE ions with a relatively large radius, ranging from 0.868 to 1.36 Å, induce larger spacing and lattice parameters in the final network. This interplay between the viscosity

Table 2 Film thicknesses evaluated by RBS analysis. Uncertainty is about 5 nm

	Sample	Thickness D (nm)
Na series	Na10Eu5	320
	Na20Eu5	315
	Na30Eu5	350
Eu series	Na20Eu0	Not measurable
	Na20Eu1	Not measurable
	Na20Eu2	190
	Na20Eu5	315
	Na20Eu8	415

Tab 3 Photoluminescence data reporting the integrated intensity I_{PL}, the normalized integrated intensity I_{PL}/Eu, the measured PL decay lifetime τ_{EXP}, the symmetry factor R, the radiative lifetime τ_{RAD} and the quantum efficiency $QY = \tau_{\mathrm{EXP}}/\tau_{\mathrm{RAD}}$. Relative uncertainty of the data is below 5%

Sample	Int. PL ex. 393 nm (arb. units)	I_{PL}/Eu ex. 393 nm	Na series Lifetime τ_{EXP} (ms)	Symmetry R-factor	Radiative lifetime τ_{RAD} (ms)	Quantum efficiency QY (%)
Na10Eu5	96	19	1.71	3.4	3.37	51
Na20Eu5	115	23	2.09	3.7	3.28	64
Na30Eu5	122	24	2.29	3.6	3.47	66
Sample	Int. PL ex. 393 nm (arb. units)	I_{PL}/Eu ex. 393 nm	Eu series Lifetime τ_{EXP} (ms)	Symmetry R-factor	Radiative lifetime τ_{RAD} (ms)	Quantum efficiency QY (%)
Na20Eu1	22	22	1.70	2.2	3.38	50
Na20Eu2	33	17	2.01	2.6	3.50	57
Na20Eu5	115	23	2.09	3.7	3.28	64
Na20Eu8	261	33	2.16	4.2	3.07	71

of the solution, the increase in porosity and the incorporation of larger dopants results in thicker films at higher Eu concentrations, as observed by other authors too [39].

Photoluminescence characterizations are reported in Fig. 3 for Na series (left) and Eu series (right) samples, while Table 3 contains the main optical data obtained from them: the integrated intensity, the normalized integrated intensity, the measured PL decay lifetime τ_{EXP}, the symmetry factor R, the radiative lifetime τ_{RAD} and the quantum efficiency QY. Photoluminescence excitation spectra (PLE) are reported in panel (a) and (b). The absorption transitions from the $^7F_0$ ground level to the upper energy levels are clearly observed. The most intense is the $^7F_0 \rightarrow {}^7L_6$ at 393 nm, which was thus chosen as excitation for the PL emission. The PL emission spectra in panel (c) and (d) show the typical peaks related to the $^5D_0 \rightarrow {}^7F_J$ manyfold ($J = 0$–6) with maximum PL intensity at 611 nm, corresponding to the $^5D_0 \rightarrow {}^7F_2$ transition. As previously discussed, the analysis of the spectral shape of the emission allows for Eu^{3+} ions the calculation of the symmetry factor R and radiative lifetime τ_{RAD}, which are reported in Table 3. The symmetry factor is related to the local environment surrounding Eu^{3+} ions. The higher this factor, the lower the local symmetry around Eu^{3+} is with respect to an inversion center, resulting in a stronger PL emission. It can be observed that Na concentration from 10 to 30 at% has a limited impact on the site symmetry of Eu^{3+} ions (in the range $3.4 \div 3.7$). Instead, the symmetry factor depends significantly on the increasing concentration of Eu atoms from 1 to 8 at%, rising from 2.2 to 4.2. This is a further indication of the role of Eu as structural modifier for the glass network. The radiative lifetime τ_{RAD} was also calculated from the spectral shape. The values range from 3.10 to 3.50 ms, without a definite trend with Na or Eu concentrations.

The normalized time-resolved PL decay is shown in panels (e) and (f) in linear-log scale to highlight the exponential decrease that is typical of spontaneous transitions from the excited states to the lower lying energy levels [40]. To account for different sites and inhomogeneous distributions, the decay curves were fitted with a double exponential equation:

$$I(t) = I_0 + A_1 e^{-\frac{t}{\tau_1}} + A_2 e^{-\frac{t}{\tau_2}} \tag{5}$$

where $I(t)$ is the normalized emission intensity as a function of time t, I_0 is a constant related to the background, A_1 and A_2 are the amplitude contributions, and τ_1 and τ_2 are the fast and slow lifetime components, respectively. The experimental lifetime, also listed in Table 3, is calculated as the weighted average of the two components, given by the following equation [40]:

$$\tau_{\mathrm{EXP}} = \frac{A_1\tau_1^2 + A_2\tau_2^2}{A_1\tau_1 + A_2\tau_2} \tag{6}$$

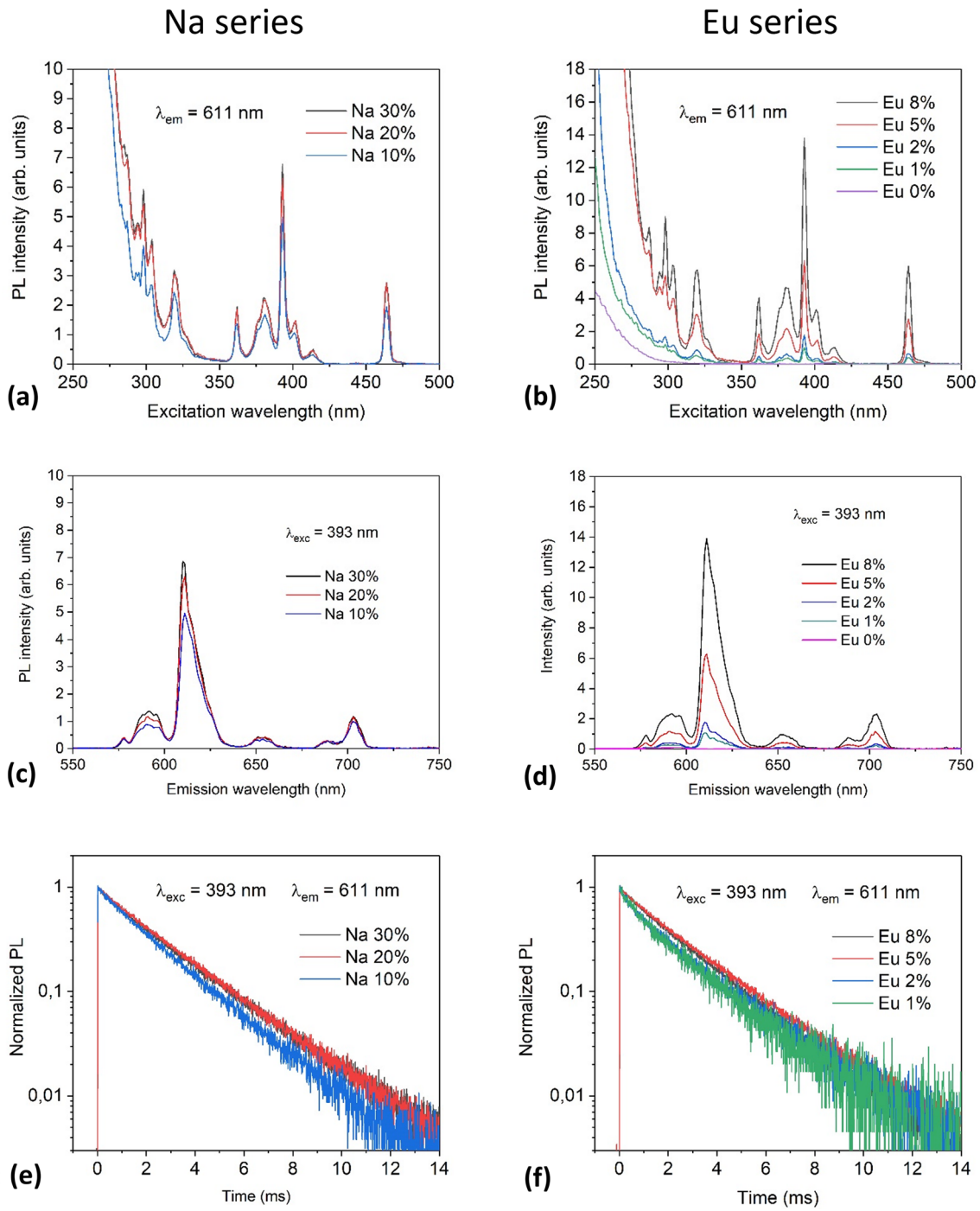

Fig. 3 Photoluminescence characterization for Na series (left) and Eu series (right) samples. Excitation spectra (**a**) (**b**), emission spectra (**c**) (**d**), time-resolved PL decay (**e**) (**f**)

As previously discussed, the quantum efficiency QY of the system can be evaluated by the rate between the experimental lifetime and the radiative lifetime. It is worth observing that both the experimental lifetimes and the quantum efficiencies increase by increasing Na and/or Eu content in the films. For Na series, the quantum efficiencies rise from about 51 to 66%. A reasonable explanation is the better dispersion and lower clustering of RE ions with increase in Na, as predicted by molecular dynamic simulations, lowering non-radiative recombination processes. In Eu series, the quantum efficiencies rise from 50 to 71%, confirming the role of Eu^{3+} in improving the structural quality of the network.

As a final analysis, the integrated PL emissions as a function of Na content and Eu content are reported in Fig. 4a and b, respectively. From a theoretical point, the PL intensity is proportional to the density of emitters, the thickness D of the film and

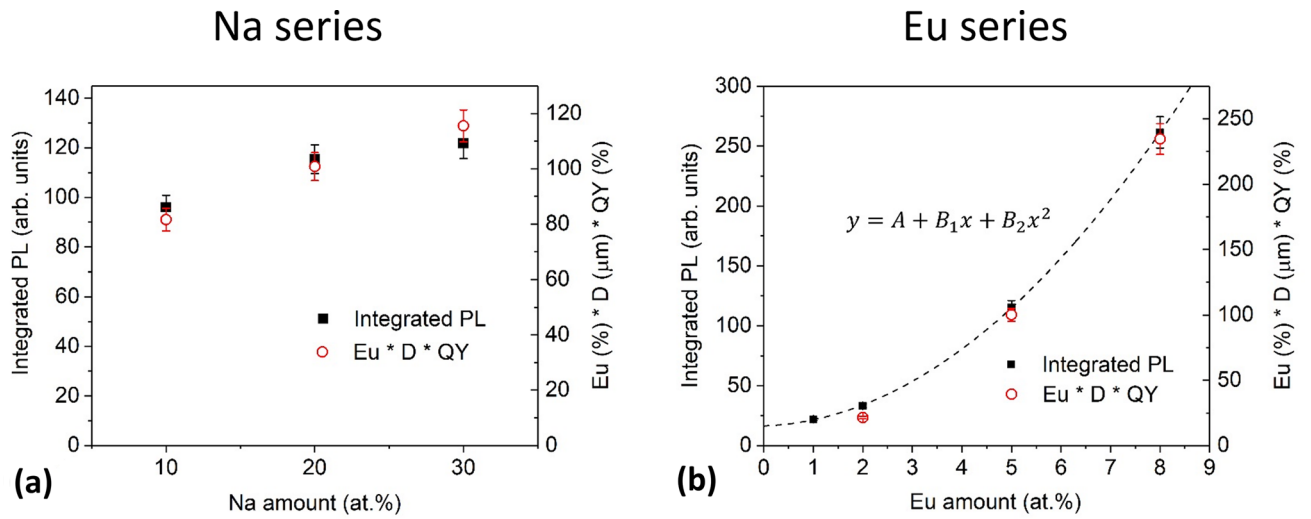

Fig. 4 Integrated PL intensity for Na series (**a**) and Eu series (**b**) samples (black squares) compared to the product of Eu concentration, thickness D and QY (red circles)

the QY of the emitters. In the same graphs, the product of these factors is reported with red circles. In the first graph, panel (a), an increasing trend (about 25%) can be observed with Na increase. This improvement can be reasonably attributed to the better structural environment for RE atoms due to the presence of sodium, as reflected by the observed increase of QY from 51 to 66%. In the second graph, panel (b), related to Eu concentration, the trend exhibits a nonlinear behavior, as attested by the excellent second order polynomial fit. This is in perfect agreement with the increase of the number of emitting species, the increase of the sample thicknesses and the increase of the quantum efficiencies. It is also remarkable that no concentration quenching is observed for Eu concentrations as high as 8 at%.

6 Conclusions

This paper is focused on sol–gel Eu-doped silica–soda glasses. According to molecular dynamic simulations, the addition of soda to silica can reduce RE clustering and precipitation. It was shown that increasing Na content from 10 to 30 at% increases the PL intensity. Moreover, Eu plays a significant role, too, in the structural and optical properties of the system. Increasing Eu concentration improves the transparency, the refractive index and the thickness of the films, together with a quadratic increase of PL emission. The optical characterization analysis revealed a decrease of site symmetry (increase of the symmetry R-factor) and an increase of quantum efficiency (QY), reaching 71% for the highest 8 at% doping, attributed to the better structural environment surrounding Eu^{3+} ions. The total PL emission was successfully related to the combined contribution of Eu concentration, film thickness and QY of the emitters, reporting the remarkable absence of concentration quenching for Eu doping as high as 8 at% in this system.

Funding Open access funding provided by Università degli Studi di Verona within the CRUI-CARE Agreement. F.E. acknowledges VINNOVA for financial support through the Vinnmer Marie Curie Project "Nano2solar"; F.E. and G.C.R. acknowledge MAECI for financial support through the PLESC project between South Africa and Italy; A.V. acknowledges MUR for financial support through the PNRR NEST network.

Data Availability Statement This manuscript has associated data in a data respiratory. [Authors' comment: Data will be made available on reasonable request.]

Declarations

Conflict of interests Nothing to declare.

References

1. E. Desurvire, Erbium-doped fiber amplifiers: principles and applications, New York, 1994.
2. M.J.F. Digonnet, Rare-earth-doped fiber lasers and amplifiers, revised and expanded, rare-earth-doped fiber lasers and amplifiers. Revis. Expanded. (2001). https://doi.org/10.1201/9780203904657
3. T. Trupke, M.A. Green, P. Würfel, Improving solar cell efficiencies by down-conversion of high-energy photons. J. Appl. Phys. **92**, 1668–1674 (2002). https://doi.org/10.1063/1.1492021
4. T. Trupke, M.A. Green, P. Würfel, Improving solar cell efficiencies by up-conversion of sub-band-gap light. J. Appl. Phys. **92**, 4117–4122 (2002). https://doi.org/10.1063/1.1505677
5. A. Bouajaj, S. Belmokhtar, M.R. Britel, C. Armellini, B. Boulard, F. Belluomo, A. Di Stefano, S. Polizzi, A. Lukowiak, M. Ferrari, F. Enrichi, Tb3+/Yb3+ codoped silica-hafnia glass and glass-ceramic waveguides to improve the efficiency of photovoltaic solar cells. Opt. Mater. (Amst). **52**, 62–68 (2016). https://doi.org/10.1016/j.optmat.2015.12.013
6. F. Enrichi, C. Armellini, S. Belmokhtar, A. Bouajaj, A. Chiappini, M. Ferrari, A. Quandt, G.C. Righini, A. Vomiero, L. Zur, Visible to NIR downconversion process in Tb3+-Yb3+codoped silica-hafnia glass and glass-ceramic sol-gel waveguides for solar cells. J. Lumin. **193**, 44–50 (2018). https://doi.org/10.1016/j.jlumin.2017.08.027
7. L. Zur, C. Armellini, S. Belmokhtar, A. Bouajaj, E. Cattaruzza, A. Chiappini, F. Coccetti, M. Ferrari, F. Gonella, G.C. Righini, E. Trave, A. Vomiero, F. Enrichi, Comparison between glass and glass-ceramic silica-hafnia matrices on the down-conversion efficiency of Tb3+/Yb3+ rare earth ions. Opt. Mater. (Amst). **87**, 102–106 (2019). https://doi.org/10.1016/j.optmat.2018.05.008
8. G.C. Righini, F. Enrichi, L. Zur, M. Ferrari, Rare-earth doped glasses and light managing in solar cells. J. Phys. Conf. Ser. **1221**, 012028 (2019). https://doi.org/10.1088/1742-6596/1221/1/012028
9. E. Erol, N. Vahedigharehchopogh, O. Kıbrıslı, M.Ç. Ersundu, A.E. Ersundu, Recent progress in lanthanide-doped luminescent glasses for solid-state lighting applications—a review. J. Phys. Condens. Matter **33**, 483001 (2021). https://doi.org/10.1088/1361-648X/ac22d9
10. M. Djamal, L. Yuliantini, R. Hidayat, K. Boonin, P. Yasaka, J. Kaewkhao, Glass medium doped rare earth for sensor material, Mater Today Proc. 5 (2018) 15126–15130. www.sciencedirect.comwww.materialstoday.com/proceedings2214-7853. Accessed October 6, 2023.
11. G. Liu, B. Jacquier (eds), Spectroscopic properties of rare earths in optical materials. Springer-Verlag, Berlin (2006). https://doi.org/10.1007/3-540-28209-2.
12. K. Arai, H. Namikawa, K. Kumata, T. Honda, Y. Ishii, T. Handa, Aluminum or phosphorus co-doping effects on the fluorescence and structural properties of neodymium-doped silica glass. J. Appl. Phys. **59**, 3430–3436 (1986). https://doi.org/10.1063/1.336810
13. R.S. Quimby, W.J. Miniscalco, B. Thompson, Clustering in erbium-doped silica glass fibers analyzed using 980 nm excited-state absorption. J. Appl. Phys. **76**, 4472–4478 (1994). https://doi.org/10.1063/1.357278
14. M. Cassetta, G. Mariotto, N. Daldosso, E. De Bona, M. Biesuz, G.D. Sorarù, R. Almeev, M. Zanatta, F. Vetere, Viscosity, boson peak and elastic moduli in the Na_2O-SiO_2 system. Minerals. **13** (2023). https://doi.org/10.3390/min13091166.
15. C. Le Losq, A.P. Valentine, B.O. Mysen, D.R. Neuville, Structure and properties of alkali aluminosilicate glasses and melts: Insights from deep learning. Geochim. Cosmochim. Acta **314**, 27–54 (2021). https://doi.org/10.1016/J.GCA.2021.08.023
16. P.M. Peters, S.N. Houde-Walter, Local structure of Er3+ in multicomponent glasses. J. Non Cryst. Solids **239**, 162–169 (1998). https://doi.org/10.1016/S0022-3093(98)00733-9
17. S. Tanabe, Optical transitions of rare earth ions for amplifiers: how the local structure works in glass. J. Non Cryst. Solids **259**, 1–9 (1999). https://doi.org/10.1016/S0022-3093(99)00490-1
18. D. Levy, R. Reisfeld, D. Avnir, Fluorescence of europium(III) trapped in silica gel-glass as a probe for cation binding and for changes in cage symmetry during gel dehydration. Chem. Phys. Lett. **109**, 593–597 (1984). https://doi.org/10.1016/0009-2614(84)85431-7
19. S.K. Gupta, B. Rajeshwari, S.N. Achary, S.J. Patwe, A.K. Tyagi, V. Natarajan, R.M. Kadam, Europium luminescence as a structural probe: structure-dependent changes in Eu3+-substituted Th(C2O4)2 xH2O (x = 6, 2, and 0). Eur. J. Inorg. Chem. **2015**, 4429–4436 (2015). https://doi.org/10.1002/ejic.201500623
20. D.V. Deyneko, I.V. Nikiforov, D.A. Spassky, YYu. Dikhtyar, S.M. Aksenov, SYu. Stefanovich, B.I. Lazoryak, Luminescence of Eu3+ as a probe for the determination of the local site symmetry in β-Ca3(PO4)2-related structures. CrystEngComm **21**, 5235–5242 (2019). https://doi.org/10.1039/C9CE00931K
21. R. Reisfeld, E. Zigansky, M. Gaft, Europium probe for estimation of site symmetry in glass films, glasses and crystals. Mol. Phys. **102**, 1319–1330 (2004). https://doi.org/10.1080/00268970410001728609
22. R. Marin, G. Sponchia, E. Zucchetta, P. Riello, F. Enrichi, G. De Portu, A. Benedetti, Monitoring the t → m martensitic phase transformation by photoluminescence emission in Eu3+-doped zirconia powders. J. Am. Ceram. Soc. **96**, 2628–2635 (2013). https://doi.org/10.1111/jace.12363
23. C. Malba, U.P. Sudhakaran, S. Borsacchi, M. Geppi, F. Enrichi, M.M. Natile, L. Armelao, T. Finotto, R. Marin, P. Riello, A. Benedetti, Structural and photophysical properties of rare-earth complexes encapsulated into surface modified mesoporous silica nanoparticles. Dalton Trans. **43**, 16183–16196 (2014). https://doi.org/10.1039/c4dt00760c
24. M.H.V. Werts, R.T.F. Jukes, J.W. Verhoeven, The emission spectrum and the radiative lifetime of Eu3+ in luminescent lanthanide complexes. Phys. Chem. Chem. Phys. **4**, 1542–1548 (2002). https://doi.org/10.1039/b107770h
25. F. Enrichi, Investigation and modelling of the energy transfer between Si or Ag nanostructures and erbium ions for optical amplification. PhD Thesis (2005).
26. J. Du, L. Kokou, Europium environment and clustering in europium doped silica and sodium silicate glasses. J. Non Cryst. Solids **357**, 2235–2240 (2011). https://doi.org/10.1016/j.jnoncrysol.2010.11.088
27. B.R. Judd, Optical absorption intensities of rare-earth ions. Phys. Rev. **127**, 750–761 (1962). https://doi.org/10.1103/PhysRev.127.750
28. G.S. Ofelt, Intensities of crystal spectra of rare-earth ions. J. Chem. Phys. **37**, 511–519 (1962). https://doi.org/10.1063/1.1701366
29. L.R. Doolittle, Algorithms for the rapid simulation of Rutherford backscattering spectra. Nucl Instrum Methods Phys Res B. **9**, 344–351 (1985). https://doi.org/10.1016/0168-583X(85)90762-1
30. C.F. Bohren, D.R. Huffman, Absorption and scattering of light by small particles. Wiley, New York (1998). https://doi.org/10.1002/9783527618156
31. I. Saidi, S. Jacques, F. Tittel, Mie and Rayleigh modeling of visible-light scattering in neonatal skin. Appl. Opt. **34**, 7410–7418 (1995). https://doi.org/10.1364/AO.34.007410
32. V. Tuchin, Polarized light interaction with tissues. J. Biomed. Opt. **21**, 071114 (2016). https://doi.org/10.1117/1.JBO.21.7.071114
33. P. Chimalawong, K. Kirdsiri, J. Kaewkhao, P. Limsuwan, investigation on the physical and optical properties of Dy3+ doped soda-lime-silicate glasses. Procedia Eng. **32**, 690–698 (2012). https://doi.org/10.1016/j.proeng.2012.01.1328
34. P. Loiko, N. Ismail, J.D.B. Bradley, M. Götelid, M. Pollnau, Refractive-index variation with rare-earth incorporation in amorphous Al2O3 thin films. J. Non Cryst. Solids **476**, 95–99 (2017). https://doi.org/10.1016/j.jnoncrysol.2017.09.033

35. G.H. Frischat, Sodium diffusion in SiO_2 glass. J. Am. Ceram. Soc. **51**, 528–530 (1968). https://doi.org/10.1111/j.1151-2916.1968.tb15681.x
36. S.I. Sviridov, Z.G. Tyurnina, N.G. Tyurnina, Diffusion of alkali cations in two-component oxide glasses. Glass Phys. Chem **46**, 526–530 (2020). https://doi.org/10.1134/S1087659620060267
37. W. Haller, D.H. Blackburn, J.H. Simmons, Miscibility gaps in alkali-silicate binaries—data and thermodynamic interpretation. J. Am. Ceram. Soc. **57**, 120–126 (1974). https://doi.org/10.1111/J.1151-2916.1974.TB10832.X
38. R.M. Almeida, M.C. Gonçalves, Crystallization of solgel-derived glasses. Int. J. Appl. Glass Sci. **5**, 114–125 (2014). https://doi.org/10.1111/IJAG.12075
39. A. Abdullah, E.M. Benchafia, D. Choi, S. Abedrabbo, Synthesis and characterization of erbium-doped silica films obtained by an acid–base-catalyzed sol–gel process. Nanomaterials **13**, 1508 (2023). https://doi.org/10.3390/nano13091508
40. J.R. Lakowicz, Principles of fluorescence spectroscopy. Springer-Verlag, Boston (2006). https://doi.org/10.1007/978-0-387-46312-4